

Breast Mass Segmentation and Shape Classification in Mammograms Using Deep Neural Networks

Vivek Kumar Singh, Hatem A. Rashwan, Santiago Romani, Farhan Akram, Nidhi Pandey, Md. Mostafa Kamal Sarker, Adel Saleh, Meritxell Arenas, Miguel Arquez, Domenec Puig, Jordina Torrents-Barrena

Abstract—Mammogram analysis to manually extract breast masses is a tough assignment that radiologists must frequently carry out. Therefore, image analysis methods are needed for the detection and delineation of breast masses, which portray crucial morphological information that will support reliable diagnosis. In this paper, we proposed a conditional Generative Adversarial Network (cGAN) devised to segment a breast mass within a region of interest (ROI) in a mammogram. The generative network learns to recognize the breast mass area and to create the binary mask that outlines the breast mass. In turn, the adversarial network learns to distinguish between real (ground truth) and synthetic segmentations, thus enforcing the generative network to create binary masks as realistic as possible. The cGAN works well even when the number of training samples are limited. Therefore, the proposed method outperforms several state-of-the-art approaches. This hypothesis is corroborated by diverse experiments performed on two datasets, the public *INbreast* and a private in-house dataset. The proposed segmentation model provides a high Dice coefficient and Intersection over Union (IoU) of 94% and 87%, respectively. In addition, a shape descriptor based on a Convolutional Neural Network (CNN) is proposed to classify the generated masks into four mass shapes: irregular, lobular, oval and round. The proposed shape descriptor was trained on *Digital Database for Screening Mammography (DDSM)* yielding an overall accuracy of 80%, which outperforms the current state-of-the-art.

Index Terms—Mammograms, conditional generative adversarial network, convolutional neural network, mass segmentation and shape classification.

I. INTRODUCTION

Breast cancer is the most common diagnosed cause of death from cancer in women in the world [1]. Mammography is a world recognized tool that has been proven effective to reduce the mortality rate, since it allows early detection of breast diseases [2].

Breast masses are the most important findings among diverse types of breast abnormalities, such as micro-calcification and architectural distortion, as they may point out the presence of carcinomas [3]. Expert radiologists are needed to analyze the ROI, which is costly and time consuming job. Therefore, computer aided diagnosis (CAD) systems are highly recommended to assist radiologists in detecting breast masses

V. K. Singh, H. A. Rashwan, S. Romani, N. Pandey, M. M.K. Sarker, A. Saleh, D. Puig, J. Torrents-Barrena: Universitat Rovira i Virgili, Spain
F. Akram: Imaging Informatics Division, Bioinformatics Institute, A*STAR, Singapore.
M. Arenas and M. Arquez: Hospital Sant Joan de Reus, Spain

This work has been submitted to the IEEE for possible publication. Copyright may be transferred without notice, after which this version may no longer be accessible.

and outlining borders. Moreover, morphological information of mass shape (irregular, lobular, oval, round) and margin type (circumscribed, ill defined, spiculated, obscured) also play crucial roles in the diagnosis of mass malignancy [4].

Breast mass segmentation and classification are challenging problems due to low signal-to-noise ratio and variability of masses in shape, size, appearance, texture and location. In this paper, we propose a two stage breast mass segmentation and classification method. In the first stage, our method segments the breast mass as a binary mask. In the second stage, the binary mask is classified to a shape type. Unlike traditional object classifiers [5], [6] that use texture, intensity or edge information, our method is forced to learn only morphological features. The major contributions of this paper are as follows:

- 1) We believe this is the first adaptation of cGAN in the area of breast mass segmentation in mammograms. The adversarial network yields more reliable learning than other state-of-the-art algorithms since training data is scarce (*e.g.*, mammograms with labeled breast mass boundaries), while it does not increase the computational complexity at prediction time.
- 2) The implementation of a multi-class CNN architecture to predict the four breast mass shapes (*i.e.*, irregular, lobular, oval and round) using the binary mask segmented in the previous stage (cGAN output).
- 3) An in-depth evaluation of our system's performance using two public (1,274 images) and one private (300 images) databases. The obtained results outperform current state-of-the-art in both mass segmentation and shape classification.

This paper is organized as follows. Section II provides the related work. The proposed architectures for mass segmentation (using cGAN) and shape classification (using CNN) are described in Section III. To be more specific, in this section, we extend our previous work [7] by modifying the cGAN generator loss. The cGAN architecture is adapted to learn explicit and contextual features of the breast mass boundaries. An exploration of the CNN classifier in terms of kernel sizes, number of filters and layers is also performed. Furthermore, the whole pipeline (see Fig. 1) is enhanced with pre- and post-processing methodologies. In Section IV, extensive experiments are performed on the two stages of the proposed method and the obtained results are compared with the state-of-the-art results. For the segmentation stage, our method is compared with 4 recent works and 8 image-

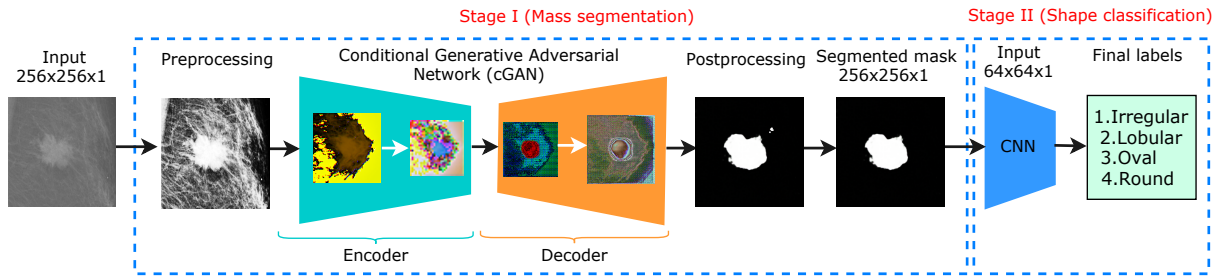


Fig. 1: General framework of breast mass segmentation and shape classification.

based segmentation models. Also, our classification method is compared with 4 recent similar works. Finally, Section V concludes our work and suggests some future lines of research.

II. RELATED WORK

A. Mass Segmentation Background

Convolutional Neural Networks (CNNs) can automatically learn features from the given images to represent objects at different scales and orientations. By increasing the number of layers (depth of CNN model) more detailed features can be obtained, which play crucial part in solving different computer vision problems, such as object detection, classification and segmentation. Thus, numerous methods has been proposed to solve the image segmentation problem based on deep learning approaches [8]. One of the well-known architectures for semantic segmentation is the Fully Convolutional Network (FCN) [9], which is based on encoding (convolutional) and decoding (deconvolutional) layers. This approach gets rid of the fully connected layers of CNNs to convert the image classification networks into image filtering networks. An improvement of this scheme was proposed by the U-Net architecture [10], where skip connections between encoding and decoding layers are added to retain significant information from the input features. Later on, a new variation of FCN was proposed [11] named SegNet, which consists of hierarchy of decoders, each one corresponding to each encoder. The decoder network uses the max-pooling indices received from the corresponding encoder to perform non-linear upsampling of their input feature maps.

Since semantic segmentation has achieved great progress with deep learning, there is recent popularity in applying such models to medical imaging [12]. For instance, to segment skin lesions on dermoscopic images, the SLSDeep model [13] was proposed to upscale the feature maps from the encoding layers at multi-scale to preserve small details (e.g., lesion borders). In [14], a multi-scale deep model with multi-level loss was proposed for segmenting optic disk and cup in Fundus images. Many segmentation approaches can be trained from scratch [15] but also can reuse the weights obtained for the starting CNN layers of other architectures such as ResNet [16] and VGG [17] trained on ImageNet data [18].

Regarding breast mass segmentation, many works have been proposed. A mass classification and segmentation method was proposed [19] using an automated region growing algorithm whose threshold was obtained by a trained Artificial Neural

Network (ANN) and Cellular Neural Network (CeNN). In turn, to reduce the computational complexity and increase the robustness, a quantized and non-linear CeNN for breast mass segmentation was proposed in [20]. After segmenting the breast mass region, a multilayer perceptron classifier was used for mass classification as benign or malignant.

Furthermore, Dhungel et al. [21] segmented breast masses using Structured Support Vector Machines (SSVM) and Conditional Random Fields (CRF). Both graphical models minimize a loss function build on pixel probabilities provided by a CNN and deep belief network, a Gaussian mixture model (GMM) and shape prior. The SSVM is based on graph cuts and the CRF relies on tree re-weighted belief propagation with truncated fitting training [22]. Cardoso et al. [23], [24] tackled the same problem by employing a closed contour fitting in the mammogram and minimizing a cost function depending on the radial derivative of the contour. A measure of regularity of the gray pixel values inside and outside the mass was also included in [24].

In turn, Zhu et al. [25] proposed an FCN concatenated to a CRF layer to impose the compactness of the segmentation output taking into account pixel position. This approach was trained end-to-end, since the CRF and FCN can exchange data in the forward-backward propagation. An adversarial term was introduced to prevent the samples with the worst perturbation in the loss function, which reduced the overfitting and provided a robust learning with few training samples. In addition, Alantari et al. [26] proposed a CAD system consisting of three deep learning stages for detecting, segmenting, and classifying the masses in mammographic images. To locate masses in a full mammogram, the YOLO network proposed in [27] was used. A Full resolution convolutional network (FrCN) was then used for segmenting the located mass region. Finally, A CNN network was used for classifying segmented ROI as either benign or malignant.

We believe [28] is the first work that exploits GAN [29] for medical image segmentation, in particular three-dimensional (3D) liver segmentation using abdominal computerized tomography (CT) scans. In [7], we adapted a cGAN image-to-image translation algorithm [30] to address the mass segmentation in two-dimensional (2D) mammograms. Our system provided state-of-the-art performance on both public and private databases.

B. Shape Classification Background

In the literature, many approaches focused on deep learning architectures have recently been designed for 2D and 3D shape classification [31]. For example, topological data analysis (TDA) using deep learning was proposed in [32] to extract relevant 2D/3D topological and geometrical information. In turn, a CNN model was formulated, which uses spectral graph wavelets in conjunction with the bag of features paradigm to target the shape classification problem [33]. In addition, the authors in [34] proposed a CNN based shape descriptor for retrieving the 3D shapes. A deep neural network named PointNet was proposed [35], which directly consumes point cloud for object classification, localized and global semantic segmentation. Moreover, a deep learning framework for efficient 3D shape classification was proposed [36] that uses geodesic moments by inheriting various properties from the geodesic distance, such as the intrinsic geometric structure of 3D shapes and the invariance to isometric deformations.

Hitherto, numerous shape classification methods are applied for medical image analysis [12]. Fourier shape descriptors with a CNN were used [37] to characterize the lung nodules heterogeneity in CT scans. A CNN architecture coupled with neighboring ensemble predictor invariant to the neighborhood was proposed [38] for nucleus detection and classification in histology images.

An automated method for textual description of anatomical breast mass lesions was proposed by Kisilev et al. [5], which performs joint semantic estimation from image measurements to classify the mass shape. In addition, Kisilev et al. [39] also presented a multi-task fast region-based CNN [40] to classify three mass shapes: irregular, oval and round. Furthermore, the work in [6] utilized a GAN to diagnose and classify masses in mammograms into four shapes: irregular, lobular, oval and round. Previously, Singh et al. [7] proposed a multi-class CNN to categorize the mass shapes into four classes as in [6] from the public dataset DDSM¹.

III. PROPOSED METHODOLOGY

The proposed CAD system shown in Fig. 1 is divided into two stages: breast mass segmentation and shape classification. In the first stage, mammograms are pre-processed for noise removal (Gaussian filter with $\sigma = 0.5$) and then contrast is enhanced using histogram equalization (pixel values are rescaled between [0 1]). Afterwards, the cGAN input is prepared by rescaling the image crops to 256×256 pixels containing different framing of the breast mass region (ROI): full mammogram, loose and tight frames (see Fig. 6). The prepared data is then fed to the cGAN to obtain a binary mask of the breast mass, which is post-processed using morphological operations (3×3 closing, 2×2 erosion, and 3×3 dilation) to remove small speckles. In the second stage, the output binary mask is downsampled into 64×64 pixels, which is then fed to a multi-class CNN shape descriptor to categorize it into four classes: irregular, lobular, oval and round.

A. Mass Segmentation Model (cGAN)

Our previous work [7] demonstrated the feasibility of applying the cGAN image-to-image translation approach [30] to breast mass segmentation, since it can be adapted to our problem in the following senses:

- 1) The Generator G network of the cGAN is an FCN composed of encoding and decoding layers, which learn the intrinsic features (gray-level, texture, gradients, edges, shape, etc.) of healthy and unhealthy (mass) breast tissue, and generate a binary mask according to these features.
- 2) The Discriminative D network of the cGAN assesses if a given binary mask is likely to be a realistic segmentation or not. Therefore, including the adversarial score in the loss computation of the generator strengthens its capabilities to provide a correct segmentation.

The combination of G and D networks allows robust learning with few training samples. Since the ROI image is a conditioning input for both G and D , the segmentation result is better fitted to the mass appearance. Otherwise, regular (unconditional) GAN [29] will infer the segmentation just from random noise, which will require more training iterations compared to the cGAN to obtain an acceptable segmentation result.

Fig. 2 represents the suggested architectures for G and D . The former consists of several encoding and decoding layers (see Fig. 2-top). Encoding layers are composed of a set of convolutional filters followed by batch normalization and the leaky ReLU (slope 0.2) activation function. Similarly, decoding layers are composed of a set of deconvolutional filters followed by batch normalization, dropout and ReLU.

Convolutional and deconvolutional filters are defined with a kernel of 4×4 , stride of 2×2 , which respectively downsample and upsample the activation maps by a factor of 2. Batch normalization is not applied after the first and the last convolutional filters (Cn_1 and Cn_8). After Cn_8 , the ReLU activation function is applied instead of leaky ReLU. Dropout is applied only at the first three decoding layers (Dn_1 , Dn_2 and Dn_3). There is no skip connection in the last decoding layer (Dn_8), after which the \tanh activation function is applied to generate a binary mask of the breast mass.

Moreover, skip connections are shown using dashed arrows, which concatenate the output of each pair of encoding (cyan boxes) and decoding (orange boxes) layers (e.g., $Cn_7 \parallel Dn_1$) to create the input tensor for the following decoder (e.g., Dn_2). These skip connections [10] improve the efficacy of G because the input features obtained at each encoding layer are used by the corresponding decoding layer in the creation of the output features that will finally lead to the end segmentation. Hence, there is a correlation between input and output features at different levels of detail (layers). Moreover, the back-propagation through the skip connections improves the fitting of the encoding filters for extracting the relevant features for mass segmentation, which also speeds up the optimization process.

¹<https://wiki.cancerimagingarchive.net/display/Public/CBIS-DDSM>

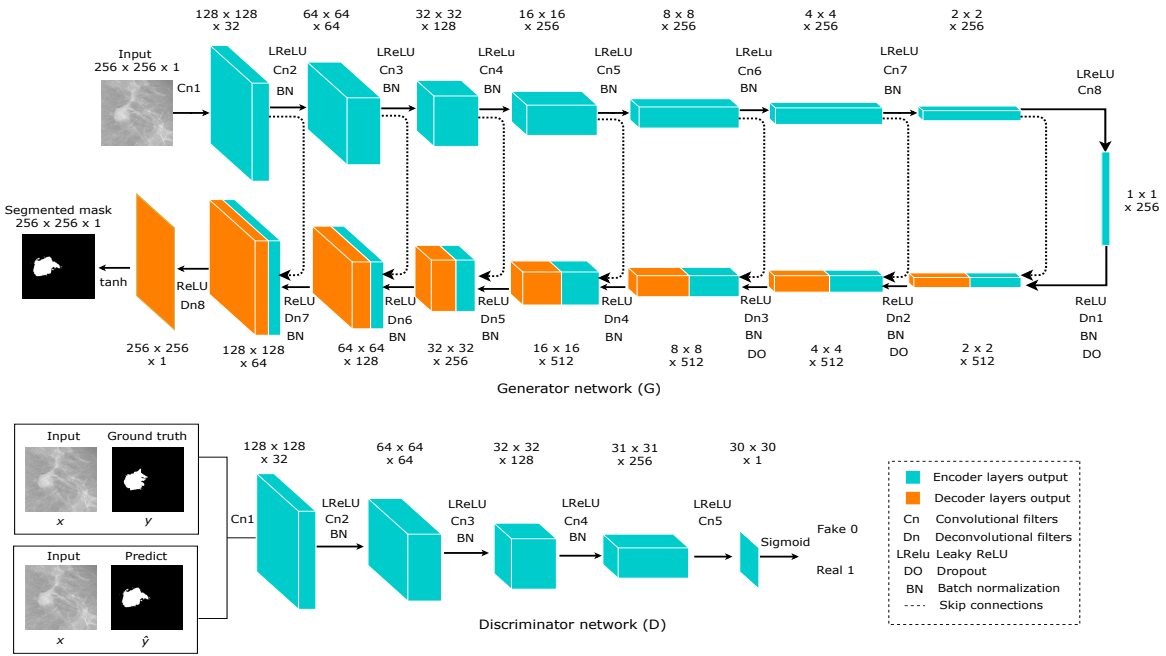


Fig. 2: Proposed cGAN architecture: generator G (top), and discriminator D (down).

The architecture of D shown in Fig. 2-down consists of five encoding layers with convolutional filters with a kernel of 4×4 , stride 2×2 at the first three layers and stride 1×1 at 4^{th} and 5^{th} layers. Batch normalization is applied after Cn_2 , Cn_3 and Cn_4 and a leaky ReLU (slope 0.2) is applied after each layer except the last. The sigmoid activation function is used after the last convolutional filter (Cn_5). The network input is the concatenation of the ROI and the binary mask to be evaluated (ground truth or predicted). The output segmentation is an array of 30×30 values, each one from 0.0 (completely fake) to 1.0 (perfectly plausible or real). Each output value is the degree of proper segmentation likelihood of a crop of the binary mask and the input image, which corresponds to the 70×70 receptive field of the value.

$$\ell_{Gen}(G, D) = \mathbb{E}_{x,y,z}(-\log(D(x, G(x, z)))) + \lambda \mathbb{E}_{x,y,z}(\ell_{Dice}(y, G(x, z))), \quad (1)$$

where z is introduced as dropout in the decoding layers Dn_1 , Dn_2 and Dn_3 at both training and testing phases, which provides stochasticity to generalize the learning processes and avoid overfitting.

The optimization process of G will try to minimize both expected values, *i.e.*, the D values should approach to 1.0 (correct mass segmentations), and the dice loss ℓ_{Dice} should approach to 0.0 (generated masks are equal to the ground truth). Both terms of the generator loss enforce the proper optimization of G : the dice loss term fosters a rough prediction of the mask shape (central mass area) while the adversarial term fosters an accurate prediction of the mask outline (mass borders). Neglecting one of the two terms may lead to either very poor segmentation results or slow learning speed.

In addition, $\ell_{Dice}(y, G(x, z))$ is the dice loss of the predicted mask with respect to the ground truth, which is defined as:

$$\ell_{Dice}(y, z) = 1 - \frac{2|y \circ G(x, z)|}{|y| + |G(x, z)|}, \quad (2)$$

where \circ is the pixel wise multiplication of the two images and $|\cdot|$ is the total sum of the pixel values of a given image. If the inputs are binary images, then each pixel can be considered as a boolean value (white is 1 / black is 0). The formulation in (2) is equivalent to the dice coefficient *i.e.*, $2 \times \frac{TP}{TP+FN+TP+FP}$, but it must be subtracted from 1.0 because the loss function will be minimized. Let A be the ground truth of the ROI and B the segmented region. Then the true positive (TP) is defined as $TP = A \cap B$, which is a set of the segmented region common in both A and B . The false positive (FP) is defined as $\bar{A} \cap B$,

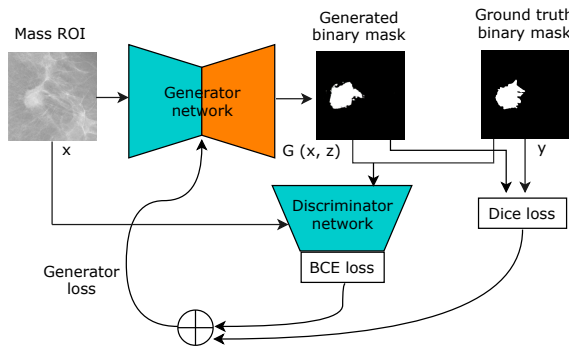


Fig. 3: Proposed cGAN framework based on dice and BCE losses.

Let x be a mass ROI, y the ground truth mask, z a random variable, λ an empirical weighting factor, $G(x, z)$ and $D(x, G(x, z))$ the outputs of G and D , respectively. Then, the loss function of G is defined as:

which is the segmented area not belonging to A . Similarly, false negative (FN) is defined as $A \cap \bar{B}$, which is the true area missed by the proposed segmentation method.

In our previous work [7], the generator network loss was formulated by combining the logistic Binary Cross Entropy (BCE) loss and the $L1$ -norm. In this work, we replace the $L1$ -norm loss with the dice loss as shown in Fig. 3. $L1$ -norm loss minimizes the sum of absolute differences between the ground truth label y and estimated binary mask G obtained from the generator network, which takes all pixels into account. In turn, dice loss is highly dependent on TP predictions (foreground region common in both ground truth and predicted region), which is the most influential term in foreground segmentation. Fig. 4 shows that the dice loss achieves lower values (more optimal) than the $L1$ -norm loss.

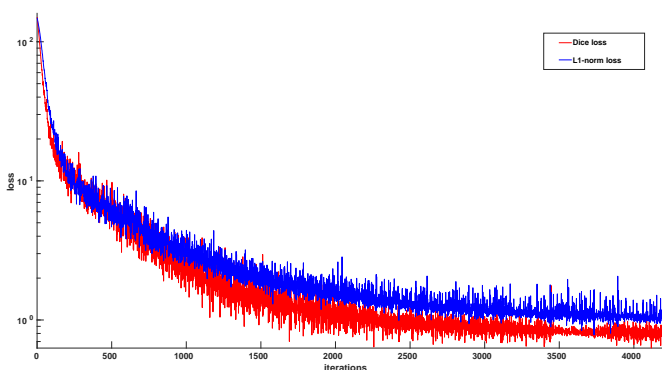


Fig. 4: Dice and L1-norm loss comparison over iterations.

Moreover, the loss function of D is defined in (3):

$$\ell_{Dis}(G, D) = \mathbb{E}_{x,y,z}(-\log(D(x,y))) + \mathbb{E}_{x,y,z}(-\log(1 - D(x,G(x,z)))) \quad (3)$$

The optimizer will fit D to maximize the loss values for ground truth masks (by minimizing $-\log(D(x,y))$) and minimize the loss values for generated masks (by minimizing $-\log(1 - D(x,G(x,z)))$). These two terms compute BCE loss using both masks, assuming that the expected class for ground truth and generated masks is 1 and 0, respectively.

The optimization of G and D is done sequentially, *i.e.*, one optimization step for both networks at each batch, where G learns how to compute a valid mass segmentations and D learns how to differentiate between synthetic and real segmentations.

In this work, we experimented on different hyper-parameters to improve the segmentation accuracy of our previous contribution in [7]. Besides the introduction of the dice loss, we reduced the number of filters of each network from 64 to 32. We also explored different learning rates and loss optimizers (SGD, AdaGrad, Adadelta, RMSProp and Adam), finding Adam with $\beta_1 = 0.5$, $\beta_2 = 0.999$ and initial learning rate = 0.0002 with batch size 8 the best combination. In (1), the dice loss weighting factor $\lambda = 150$ was found to be the best choice. Finally, better results were achieved by training both G and D from scratch for 150 epochs.

B. Shape Classification Model (CNN)

We propose a multi-class CNN architecture for breast mass shape classification (*i.e.*, irregular, lobular, oval and round) using the binary masks obtained from the cGAN. In the literature, most methods attempted to directly categorize the shape using breast mass intensity, texture, boundary, etc. ([5], [39], [40], [6]), which increase computational complexity. We simplify the problem by extracting morphological features from the binary masks.

As shown in Fig. 5, our model consists of three convolutional layers with kernel sizes 9×9 , 5×5 and 4×4 , respectively, and two fully connected (FC) layers. The first two convolutional layers are followed by 4×4 max-pooling with stride 4. The output of the last convolutional layer is flattened and then fed into the first FC layer with 128 neurons. These four layers use ReLU as an activation function. A dropout of 0.5 is used to reduce overfitting in the first FC layer. Finally, the last FC layer with 4 neurons is followed by a softmax function to generate the final membership degree of the input binary mask for each class. A weighted categorical cross-entropy loss is used to avoid the problem of unbalanced dataset. The class weight is the ratio of number of samples per class to the total samples.

The RMSProp is employed for optimizing the model with learning rate = 0.001, momentum = 0.9 and batch size = 16. The network is trained from scratch and the weights of five layers are randomly initialized. During training, we experimentally found the best architecture, number of layers, filters per layer, and number of neurons in FC layers.

IV. EXPERIMENTS AND DISCUSSION

We have evaluated the performance of the proposed models on two public mammography datasets and one private dataset: **INbreast dataset**²: it is a publicly available database containing a total of 115 cases (410 mammograms), which include: masses, calcifications, asymmetries and distortions. For testing the segmentation model, we used 106 breast mass images along with their respective ground truth binary masks.

DDSM dataset: it is a publicly available database containing 2,620 normal, benign and malignant mammograms. In this work, 1,168 cases containing benign and malignant breast masses with their corresponding ground truths are used for shape classification, where 504, 473, 115 and 76 masses are labeled as irregular, lobular, oval and round, respectively. We have used 75% of the images for training and rest for testing the mass shape classification model.

Hospital Sant Joan de Reus dataset: it is our private dataset that contains 300 malignant masses with their respective ground truth binary masks obtained by the radiologists. The proposed cGAN segmentation model is trained and tested using 220 and 80 images, respectively. The duty of confidentiality and security measures were fully complied, in accordance with the current legislation on the Protection of Personal Data (article 7.1 of the Organic Law 15/1999, 13th of December).

²http://medicalresearch.inescporto.pt/breastcancer/index.php/Get_INbreast_Database/

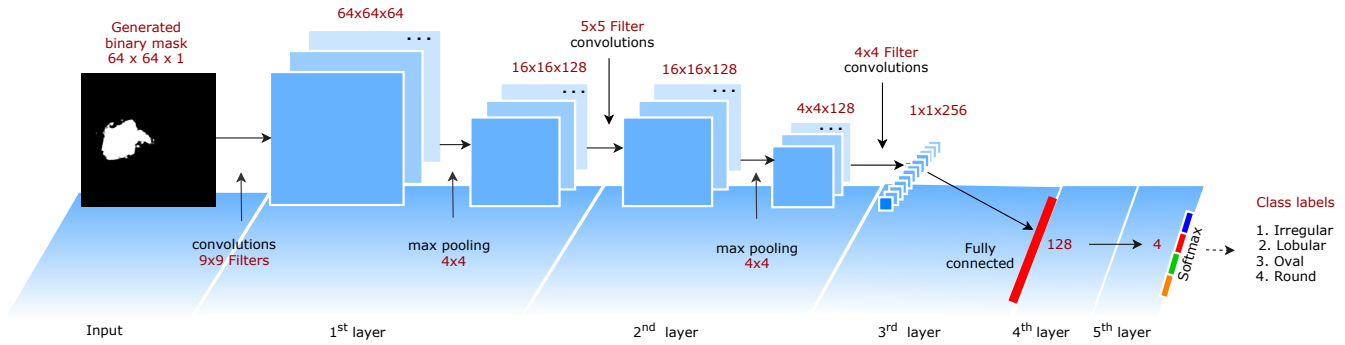


Fig. 5: CNN architecture for mass shape classification.

The proposed method was implemented using python with Pytorch³ running on a 64-bit Ubuntu operating system using a 3.4 GHz Intel Core-i7 with 16 GB of RAM and Nvidia GTX 1070 GPU with 8 GB of video RAM.

A. Mass Segmentation Experiments

The proposed breast mass segmentation method is compared with the state-of-the-art methods and evaluated both quantitatively and qualitatively. For the quantitative analysis, segmentation accuracy is computed using Dice coefficient (F1 score) and Jaccard index (IoU). In turn, for the qualitative analysis, segmentation results with their respective ground truth binary masks are compared visually.

These experiments have been carried using three different framing of the breast mass ROI: full mammogram, loose and tight frames (see Fig. 6). The ideal CAD system should be able to automatically segment the breast mass from the full mammogram. However, this is a very difficult task due to the high similarity between gray level pixel distributions of masses and healthy tissue. Therefore, removing most of the image non-ROI portions logically helps the model on learning the visual features that differentiate breast mass from non-mass areas. The loose frame provides a balanced proportion between the number of pixels of the two classes. The tight frame is intended to evaluate the behavior of the segmentation model when the majority of the image contain breast mass pixels. If the system is to be applied to new cases, an approximate frame around the breast mass must be provided, which makes the system semi-automatic, but nevertheless the mass segmentation will be very accurate (see Fig. 7 and Fig. 8).

The three cropping strategies are evaluated on our proposed cGAN and ten baseline segmentation models, referred as FCN, FCN-ResNet101, UNet, UNet-VGG16, SegNet, SegNet-VGG16, CRFCNN, SLSDeep, cGAN-ResNet101 and cGAN-ResNet101 (Dice Loss). FCN, UNet, SegNet, CNNCRF and proposed cGAN are trained from scratch. FCN-ResNet101, UNet-VGG16, SegNet-VGG16 and cGAN-ResNet101 (with and without Dice loss) are modifications of the original models, where the filters of the starting encoding layers are replaced by the starting convolutional layers of the well-known

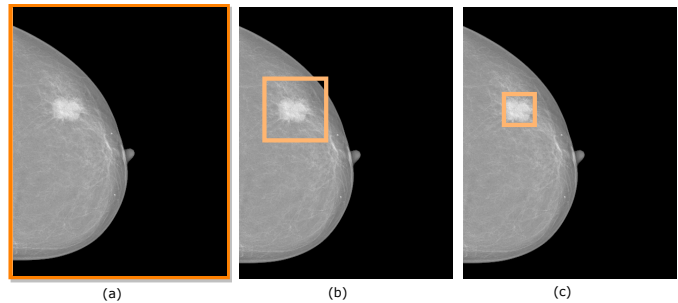


Fig. 6: Three cropping strategies: (a) full mammogram, (b) loose frame, (c) tight frame.

VGG (16 layers) and ResNet (101 layers) models, which were pre-trained on the ImageNet database. Thus, we loaded the pre-trained weights and fine tuned the network. By using the baseline model cGAN-ResNet101 [30], we replaced the L1-norm loss with the Dice loss in the generator loss function to see how the base line model will behave under such change. We called this model cGAN-ResNet101 (Dice loss) to compare the segmentation results with our proposal.

The results depicted in Table I are divided in two sections, one for our private dataset and another for the INbreast dataset. Note that all models are trained on the private dataset, and then tested to segment the breast masses using images from the INbreast dataset without fine tuning. The binary masks of breast masses in the INbreast dataset are more detailed than the ones in our private dataset.

According to the results, our method outperforms the compared state-of-the-art methods in all cases except for the IoU computed on tight crops of our private dataset. The SLSDeep approach yielded the best IoU (79.93%), whereas our method yielded the second best result (79.87%).

All models yielded their worst segmentation results for the full mammogram compared to the other frame inputs, which is logical taking into account the difficulties stated earlier in this section. Most of the models have obtained their best results for the tight frame crops except for CRFCNN and our proposal, which yielded their best results for the loose frame crops. However, the good results for tight crops may be due to the imbalance of breast mass/non-mass pixels, since the former class is present in more than 90% of the image area. The

³<https://pytorch.org/>

TABLE I: Dice and IoU metrics obtained with the proposed model and ten alternatives evaluated on the testing sets of our private and INbreast datasets, for the three cropping strategies. Best results are marked in bold. Dashes (-) indicate results not reported in the referenced papers.

Dataset	Methods	Dice (%)			IoU (%)		
		Full	Loose	Tight	Full	Loose	Tight
Private	FCN	59.06	74.94	80.20	39.92	62.21	78.89
	FCN-ResNet101	59.21	77.42	82.78	40.26	68.16	77.32
	UNet	63.69	78.03	83.15	46.73	68.36	78.81
	UNet-VGG16	59.27	78.57	83.71	42.13	69.71	79.42
	SegNet	59.87	80.26	82.33	42.79	70.07	76.17
	SegNet-VGG16	61.59	81.09	81.41	41.61	68.19	77.82
	CRFCNN	53.21	71.33	63.52	41.38	65.24	54.28
	SLSDeep	59.64	71.10	84.28	43.89	60.16	79.93
	cGAN-ResNet101	58.37	80.11	86.22	42.12	71.91	76.62
	cGAN-ResNet101 (Dice Loss)	61.49	86.57	86.37	45.90	76.32	77.26
	Proposed cGAN	66.38	89.99	88.12	49.68	81.81	79.87
INbreast	FCN	54.36	66.12	81.74	36.88	49.38	77.33
	FCN-ResNet101	51.76	83.80	82.38	38.49	72.12	78.09
	UNet	55.58	77.92	80.76	38.46	70.83	77.97
	UNet-VGG16	56.79	78.02	80.89	39.65	68.32	78.13
	SegNet	53.33	79.06	81.11	36.36	65.37	77.02
	SegNet-VGG16	56.27	80.17	81.75	39.46	66.79	78.68
	CRFCNN	52.96	73.25	65.41	40.41	67.14	57.69
	SLSDeep	60.35	75.90	85.53	44.63	61.16	80.26
	cGAN-ResNet101	54.69	87.19	89.17	37.94	77.51	82.26
	cGAN-ResNet101 (Dice Loss)	59.72	88.89	90.42	44.89	80.58	82.95
	Proposed cGAN	68.69	94.07	92.11	52.31	87.03	84.55
	Dhungal et al.[21]	-	-	90.00	-	-	-
	Cardoso et al.[24]	-	-	90.00	-	-	-
	Zhu et al.[25]	-	-	90.97	-	-	-
	Al-antari et al.[26]	-	-	92.69	-	-	86.37

learning can be biased towards this class, which makes rough solutions (almost everything is mass) to provide very high ranks of performance. Loose frame crops, on the contrary, have a more balanced proportion of pixels for both classes, which makes them ideal to learn and evaluate the model on a realistic situation: it is more convenient for the radiologist to provide a fast draw of the frame around the breast mass rather than a tight frame.

Comparing the general results for both datasets, most methods performed better on INbreast rather than the private dataset in the loose and tight columns. This effect can be explained by the fact that INbreast provides more detailed ground truths, which leads to better testing results, despite all training processes have been conducted on our private dataset.

In general, our proposal has performed well in terms of both Dice and IoU metrics. For the private dataset, in Dice/Loose frame column, our model’s percentage (89.99%) is almost 9% above the second best model, SegNet-VGG16 (81.09%). In the IoU/Loose frame column, our model’s percentage (81.81%) is almost 10% above the second best model, cGAN-ResNet101 (71.91%). For the INbreast dataset, our Loose frame results for Dice and IoU are again the best (94.07%, 87.03%), where cGAN-ResNet101 is the second best model for both metrics (87.19%, 77.51%). Thus, our model provides an improving of 7% and 10%, respectively. The fact that the second best results are obtained by the cGAN-ResNet101 model indicates that the adversarial network really helps in training the generative network. In turn, the results obtained by the cGAN-ResNet101 (Dice Loss) mixture model are in-between the cGAN-ResNet101 and our proposal, Since the Dice loss term substitution improves the accuracy of the breast mass segmentation result.

For the INbreast dataset, we have included the results mentioned in four related papers [21], [24], [25] and [26].

For these methods, we could not compute the metrics for all columns, since they have not released their source code. Our method outperformed the first three papers under similar framework conditions. However, [26] yielded better results for dice (92.69%) and IoU (86.37%) than our model in the tight frame columns. Our results in the loose frame columns surpass their results. For a fair comparison, however, it should be checked how the referenced methods would perform on loose frame crops.

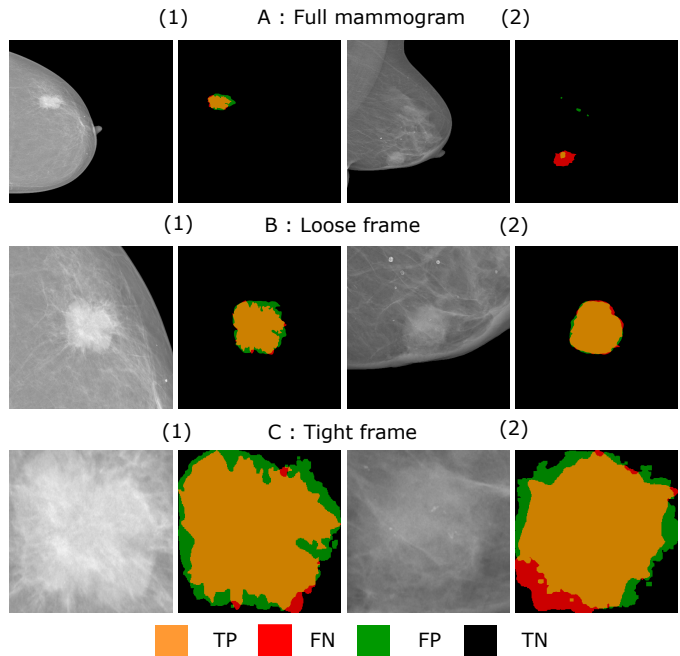


Fig. 7: Segmentation results of two testing samples extracted from the INbreast dataset with the three cropping strategies.

The high Dice and IoU metrics obtained by our model empirically prove that it performs accurate segmentations. In Fig. 7, we show some examples of our model’s segmentations using two masses from the INbreast dataset by applying the three cropping strategies. For each experiment, we show the original ROI image and the comparison of predicted and ground truth mask, color coded to mark up the true positives (TP:yellow), false negatives (FN:red), false positives (FP:green) and true negatives (TN:black). For the full mammogram, the ROI image (1) is an example of a good segmentation, since yellow and black pixels depict a high degree of confidence between predicted and real masks. On the contrary, the ROI image (2) is an example of a poor segmentation, since red pixels mark up a high portion of the breast mass area that has been misclassified as healthy area (FN). At the same time, a tiny region of green pixels shows the misclassification of healthy tissue as breast mass area (FP). Nevertheless, even in this second segmentation, there is a very high rate of black pixels (TN), which indicates that the model easily recognizes non-mass areas.

In the loose frame segmentations (middle row), specially with example (2), the results contain very few FN and FP pixels. For example (1), a modest amount of green pixels indicate that our model expands the breast mass segmentation

beyond its respective ground truth. In the tight frame crops (bottom row), besides the green areas, our model also has missed some breast mass areas *i.e.*, red pixels (FN). The mistaken areas (red and green) are mostly around the breast mass borders, since these areas have a mixture of healthy and unhealthy cells. At the same time, the inner part of the breast mass as well as the image regions outside of masses are properly classified, which indicates the stability of our model.

Fig. 8 shows a comparison between our and other six segmentation models, which work on the loose and tight frame crops using four breast masses from INbreast dataset. For the loose frame cases (four top rows), our method clearly outperforms the rest for all breast masses except for the second one, where the majority of models provided a similar degree of accuracy. In these four breast masses, UNet-VGG16 and CRFCNN provided the worst results. Moreover, cGAN-ResNet101 also performed bad in the fourth example.

For the tight frame samples (four bottom rows), our method also provides the lowest degrees of FN and FP compared to the rest of the models. Our proposed cGAN and the cGAN-ResNet101 model yield irregular borders compared to FCN-ResNet101 and SLSDeep, since GAN models strive for higher accuracy on edges. However, in the third tight frame sample (seventh row), both cGAN-ResNet101 and our proposal generated an irregular border that slightly differs from the smooth ground truth border, which results in lower segmentation accuracy around the edges. Although the rest of the models generate smoother borders, the resulting segmentations may differ from the ground truth significantly.

From the experimental results, it can be concluded that the proposed breast mass segmentation method is the most effective to date compared to the currently available state-of-the-art methods. However, our method needs a loose crop around the breast mass to obtain a proper segmentation. Moreover, our method is fast in both training and predicting *i.e.*, around 30 seconds per epoch and an image per second, respectively, which is 7 to 8 times faster than the segmentation method proposed in [26] and 10 to 15 times faster than the FCN method.

B. Shape Classification Experiments

For validating the mass shape classification performance, we computed the confusion matrix and the overall classification accuracy on the test set of the DDSM dataset. This set contains 292 images divided into: 126, 117, 31 and 18 for irregular, lobular, oval and round classes, respectively.

For the quantitative comparison, we compared our proposed model with the state-of-the-art mass shape classification methods [7], [5], [6]. The three methods were evaluated on the DDSM dataset. However, The DDSM dataset does not have the ground truth binary mask for the breast mass segmentation. Thus, we applied active contours [41], which was also used in our previous work [7], to generate the ground truths of the breast mass regions that were cropped by radiologists. Previously, [5] also used active contours [42] to generate the ground truths in a similar fashion. In addition, for reliable performance results, we used a stratified 5 fold cross validation with 50 epochs per fold.

TABLE II: Confusion matrix of the mass shape classification of testing samples of the DDSM dataset.

Prediction / Ground Truth	Irregular	Lobular	Oval	Round	Total
Irregular	96 (76%)	30	0	0	126
Lobular	33	83 (71%)	1	0	117
Oval	0	1	26 (84%)	4	31
Round	0	1	1	16 (89%)	18

In Table II, the proposed method yielded around 73% of classification accuracy for irregular and lobular classes. This result is logical, since both lobular and irregular shapes have similar irregular boundaries. In turn, our model yielded classification accuracies of 84% and 89% for oval and round shape classes, respectively.

We have computed the overall accuracy of each method by averaging the correct predictions (*i.e.*, true positive) of the four classes, weighted with respect to the number of samples per class. As shown in Table III, our classifier yields an overall accuracy of 80%, outperforming the second best results [6], [7] by 8%. In turn, Multi-task CNN [6] based on a pre-trained VGG-16 yielded the worst overall accuracy (66%), probably because the input mammograms are gray-scale images, while the VGG-16 network was trained on color-scale images.

Furthermore, the proposed shape descriptor contains 767,684 parameters, which can be trained in less than a second per epoch, and predict in about 6 milliseconds per image.

Source code of the proposed method and detailed quantitative and qualitative experimental results are given in the supplementary material.⁴

TABLE III: Shape classification overall accuracy with the DDSM dataset resulting from [5], [7], [6] and our proposed model. Best result is marked in bold.

Methods	Accuracy (%)
Kisilev et al. (SSVM) [5]	71%
Kim et al. (Multi-task CNN) [6]	66%
Kim et al. (ICADx) [6]	72%
Singh et al. [7]	72%
Proposed	80%

V. CONCLUSION

In this paper, we propose a two stage breast mass segmentation and classification method, which first segments the breast mass ROI using cGAN and then classify its binary mask using CNN based shape descriptor.

The segmentation results reveal the importance of the adversarial network in the optimization of the generative network. cGAN-ResNet101 shows an improvement of about 1% to 3% in both Dice and IoU metrics in comparison to the other non-GAN methods. In turn, the proposed method yields an increment of about 10% from the cGAN-ResNet101 by adapting the scratch model instead of ResNet101 and replacing the $L1$ -norm with the dice loss using loose frame crop on

⁴<https://drive.google.com/file/d/1DZ-0U4bXi-X42xm06aZOZWmsyysvdsY/view?usp=sharing/>

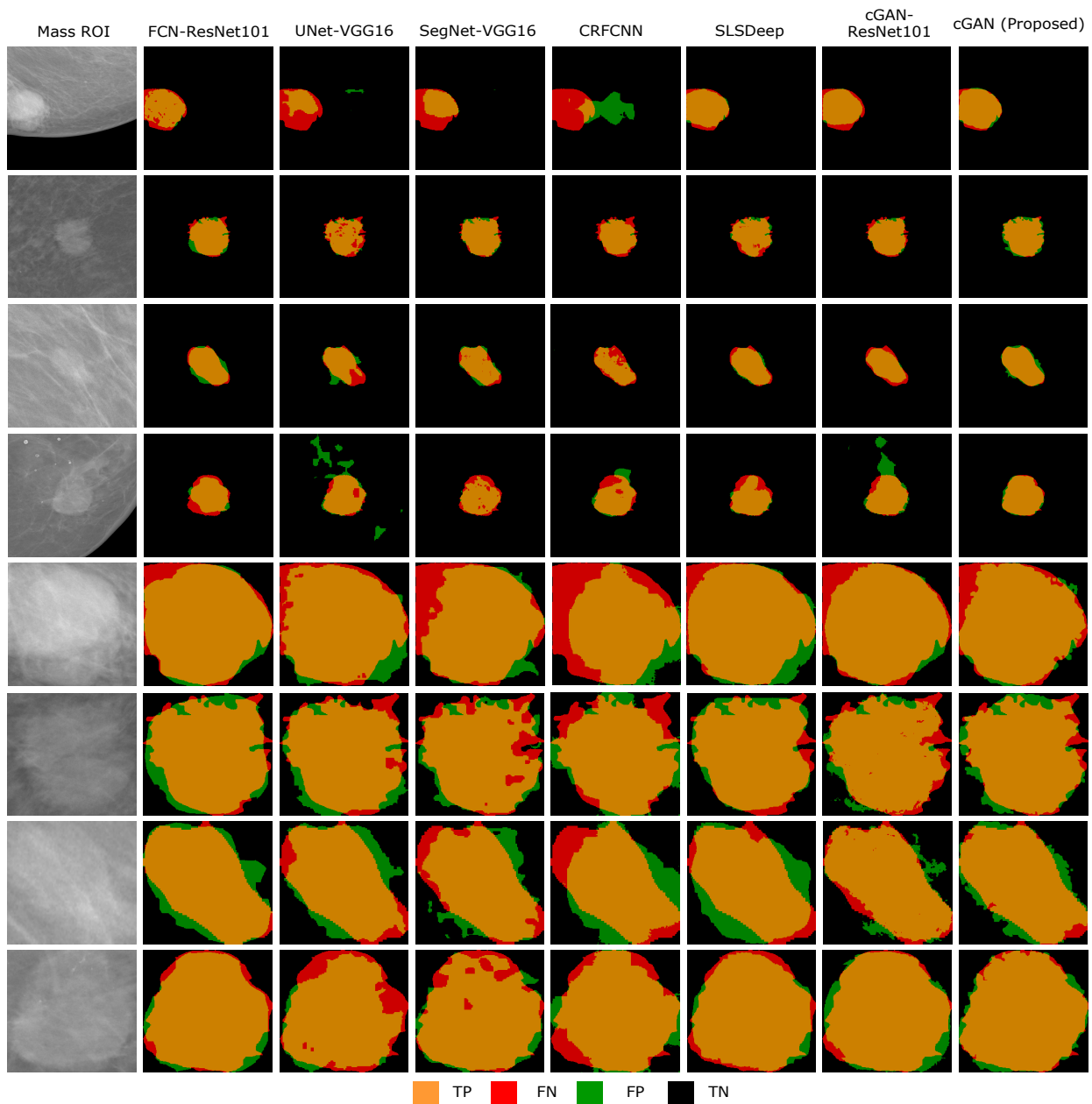


Fig. 8: Segmentation results of seven models with the INbreast dataset and two cropping strategies: loose frame (the first four rows) and tight frame (the last four rows). (Col 1) original images, (Col 2) FCN-ResNet101, (Col 3) UNet-VGG16, (Col 4) SegNet-VGG16, (Col 5) CRFCNN, (Col 6) SLSDeep, (Col 7) cGAN-ResNet101, and (Col 8) our proposed cGAN.

the given datasets. The breast mass segmentation from full-mammograms yields low segmentation accuracy for all models including the proposed cGAN. For the tight frame crop, the proposed cGAN yields similar or better segmentation accuracy compared to the other methods.

The classification results show that our second stage properly infers the mass shape from the binary mask of the breast mass, which was obtained from the first stage (cGAN segmentation). Hence, we have empirically proven that our CNN is focusing its learning on the morphological structure of the breast mass, while the rest of approaches ([5], [39], [40], [6]) rely on the original pixel variations of the input mammogram to make the same inference. Moreover, in [26]

they used a hybrid strategy in which they include the pixel variability within the mask of breast mass region to retain the intensity and texture information. However, the superior performance obtained by our method supports our initial idea that the second stage CNN can reliably recognize the breast mass shape based only on the morphological information, which is obtained from the binary mask from the segmentation stage.

Future work aims at refining our multi-stage framework to detect other breast mass features (*i.e.*, margin type, micro-calcifications), which will be integrated into a more comprehensive diagnostic to compute the degree of malignancy of the breast masses.

ACKNOWLEDGEMENTS

This work was supported by the Spanish project: DPI2016-77415-R and the Beatriu de Pinós program: 2016-BP-00063.

REFERENCES

- [1] "Breast cancer estimated incidence, mortality and prevalence worldwide in 2012. 2012."
- [2] B. Lauby-Secretan, C. Scoccianti, D. Loomis, L. Benbrahim-Tallaa, V. Bouvard, F. Bianchini, and K. Straif, "Breast-cancer screening-viewpoint of the IARC working group," *New England Journal of Medicine*, vol. 372, no. 24, pp. 2353–2358, 2015.
- [3] R. M. Rangayyan, S. Banik, and J. L. Desautels, "Computer-aided detection of architectural distortion in prior mammograms of interval cancer," *Journal of Digital Imaging*, vol. 23, no. 5, pp. 611–631, 2010.
- [4] J. Tang, R. M. Rangayyan, J. Xu, I. El Naqa, and Y. Yang, "Computer-aided detection and diagnosis of breast cancer with mammography: recent advances," *IEEE Transactions on Information Technology in Biomedicine*, vol. 13, no. 2, pp. 236–251, 2009.
- [5] P. Kisilev, E. Walach, S. Y. Hashoul, E. Barkan, B. Ophir, and S. Alpert, "Semantic description of medical image findings: structured learning approach," in *Proceedings of the British Machine Vision Conference (BMVC)*, 2015, pp. 171.1–171.11.
- [6] S. T. Kim, H. Lee, H. G. Kim, and Y. M. Ro, "ICADx: Interpretable computer aided diagnosis of breast masses," in *Proceedings of the SPIE - Medical Imaging 2018: Computer-Aided Diagnosis*, vol. 10575, 2018.
- [7] V. K. Singh, S. Romani, H. A. Rashwan, F. Akram, N. Pandey, M. M. K. Sarker, J. Torrents-Barrena, A. Saleh, M. Arenas, and D. Puig, "Conditional generative adversarial and convolutional networks for x-ray breast mass segmentation and shape classification," *CoRR*, vol. abs/1805.10207, 2018.
- [8] J. Schmidhuber, "Deep learning in neural networks: An overview," *Neural networks*, vol. 61, pp. 85–117, 2015.
- [9] J. Long, E. Shelhamer, and T. Darrell, "Fully convolutional networks for semantic segmentation," in *Proceedings of the IEEE conference on computer vision and pattern recognition (CVPR)*, 2015, pp. 3431–3440.
- [10] O. Ronneberger, P. Fischer, and T. Brox, "U-net: Convolutional networks for biomedical image segmentation," in *Proceedings of the International Conference on Medical image computing and computer-assisted intervention (MICCAI)*, 2015, pp. 234–241.
- [11] V. Badrinarayanan, A. Kendall, and R. Cipolla, "Segnet: A deep convolutional encoder-decoder architecture for image segmentation," *IEEE Transactions on Pattern Analysis and Machine Intelligence*, vol. 39, no. 12, pp. 2481–2495, 2017.
- [12] G. Litjens, T. Kooi, B. E. Bejnordi, A. A. A. Setio, F. Ciompi, M. Ghafoorian, J. A. van der Laak, B. Van Ginneken, and C. I. Sánchez, "A survey on deep learning in medical image analysis," *Medical image analysis*, vol. 42, pp. 60–88, 2017.
- [13] M. M. K. Sarker, H. A. Rashwan, F. Akram, S. F. Banu, A. Saleh, V. K. Singh, F. U. H. Chowdhury, S. Abdulwahab, S. Romani, P. Radeva, and D. Puig, "SLSDeep: Skin lesion segmentation based on dilated residual and pyramid pooling networks," *CoRR*, vol. abs/1805.10241, 2018.
- [14] H. Fu, J. Cheng, Y. Xu, D. W. K. Wong, J. Liu, and X. Cao, "Joint optic disc and cup segmentation based on multi-label deep network and polar transformation," *arXiv preprint arXiv:1801.00926*, 2018.
- [15] N. Tajbakhsh, J. Y. Shin, S. R. Gurudu, R. T. Hurst, C. B. Kendall, M. B. Gotway, and J. Liang, "Convolutional neural networks for medical image analysis: Full training or fine tuning?" *IEEE transactions on medical imaging*, vol. 35, no. 5, pp. 1299–1312, 2016.
- [16] K. He, X. Zhang, S. Ren, and J. Sun, "Deep residual learning for image recognition," in *Proceedings of the IEEE Conference on Computer Vision and Pattern Recognition (CVPR)*, 2016, pp. 770–778.
- [17] K. Simonyan and A. Zisserman, "Very deep convolutional networks for large-scale image recognition," *arXiv preprint arXiv:1409.1556*, 2014.
- [18] J. Deng, W. Dong, R. Socher, L.-J. Li, K. Li, and L. Fei-Fei, "Imagenet: A large-scale hierarchical image database," in *Computer Vision and Pattern Recognition, 2009. CVPR 2009. IEEE Conference on*. Ieee, 2009, pp. 248–255.
- [19] R. Rouhi, M. Jafari, S. Kasaei, and P. Keshavarzian, "Benign and malignant breast tumors classification based on region growing and cnn segmentation," *Expert Systems with Applications*, vol. 42, no. 3, pp. 990–1002, 2015.
- [20] Z. Liu, C. Zhuo, and X. Xu, "Efficient segmentation method using quantised and non-linear cenn for breast tumour classification," *Electronics Letters*, 2018.
- [21] N. Dhungel, G. Carneiro, and A. P. Bradley, "Deep learning and structured prediction for the segmentation of mass in mammograms," in *Proceedings of the International Conference on Medical Image Computing and Computer-Assisted Intervention (MICCAI)*, 2015, pp. 605–612.
- [22] N. Dhungel, G. Carneiro, and A. Bradley, "Tree re-weighted belief propagation using deep learning potentials for mass segmentation from mammograms," in *12th IEEE International Symposium on Biomedical Imaging, ISBI 2015, Brooklyn, NY, USA, April 16-19, 2015*, 2015, pp. 760–763.
- [23] J. S. Cardoso, I. Domingues, and H. P. Oliveira, "Closed shortest path in the original coordinates with an application to breast cancer," *International Journal of Pattern Recognition and Artificial Intelligence*, vol. 29, no. 1, 2015.
- [24] J. S. Cardoso, N. Marques, N. Dhungel, G. Carneiro, and A. Bradley, "Mass segmentation in mammograms: A cross-sensor comparison of deep and tailored features," in *Proceeding of the IEEE International Conference on Image Processing (ICIP)*, 2017, pp. 1737–1741.
- [25] W. Zhu, X. Xiang, T. D. Tran, G. D. Hager, and X. Xie, "Adversarial deep structured nets for mass segmentation from mammograms," in *Proceedings of the IEEE 15th International Symposium on Biomedical Imaging (ISBI)*, 2018, pp. 847–850.
- [26] M. A. Al-antari, M. A. Al-masni, M.-T. Choi, S.-M. Han, and T.-S. Kim, "A fully integrated computer-aided diagnosis system for digital x-ray mammograms via deep learning detection, segmentation, and classification," *International Journal of Medical Informatics*, vol. 117, pp. 44–54, 2018.
- [27] J. Redmon, S. Divvala, R. Girshick, and A. Farhadi, "You only look once: Unified, real-time object detection," in *Proceedings of the IEEE conference on computer vision and pattern recognition*, 2016, pp. 779–788.
- [28] D. Yang, D. Xu, S. K. Zhou, B. Georgescu, M. Chen, S. Grbic, D. Metaxas, and D. Comaniciu, "Automatic liver segmentation using an adversarial image-to-image network," in *Proceedings of the International Conference on Medical image computing and computer-assisted intervention (MICCAI)*, 2017, pp. 507–515.
- [29] I. Goodfellow, J. Pouget-Abadie, M. Mirza, B. Xu, D. Warde-Farley, S. Ozair, A. Courville, and Y. Bengio, "Generative adversarial nets," in *Advances in neural information processing systems*, 2014, pp. 2672–2680.
- [30] P. Isola, J.-Y. Zhu, T. Zhou, and A. A. Efros, "Image-to-image translation with conditional adversarial networks," in *Proceedings of the IEEE Conference on Computer Vision and Pattern Recognition (CVPR)*, 2017, pp. 5967–5976.
- [31] L. Kurniangggoro, K.-H. Jo *et al.*, "A survey of 2d shape representation: Methods, evaluations, and future research directions," *Neurocomputing*, vol. 300, pp. 1–16, 2018.
- [32] C. Hofer, R. Kwitt, M. Niethammer, and A. Uhl, "Deep learning with topological signatures," in *Advances in Neural Information Processing Systems*, 2017, pp. 1634–1644.
- [33] M. Masoumi and A. B. Hamza, "Spectral shape classification: A deep learning approach," *Journal of Visual Communication and Image Representation*, vol. 43, pp. 198–211, 2017.
- [34] Y. Fang, J. Xie, G. Dai, M. Wang, F. Zhu, T. Xu, and E. Wong, "3d deep shape descriptor," in *Proceedings of the IEEE Conference on Computer Vision and Pattern Recognition*, 2015, pp. 2319–2328.
- [35] C. R. Qi, H. Su, K. Mo, and L. J. Guibas, "Pointnet: Deep learning on point sets for 3d classification and segmentation," *Proc. Computer Vision and Pattern Recognition (CVPR), IEEE*, vol. 1, no. 2, p. 4, 2017.
- [36] L. Luciano and A. B. Hamza, "Deep learning with geodesic moments for 3d shape classification," *Pattern Recognition Letters*, vol. 105, pp. 182–190, 2018.
- [37] Y. Xie, J. Zhang, Y. Xia, M. Fulham, and Y. Zhang, "Fusing texture, shape and deep model-learned information at decision level for automated classification of lung nodules on chest ct," *Information Fusion*, vol. 42, pp. 102–110, 2018.
- [38] K. Sirinukunwattana, S. E. A. Raza, Y.-W. Tsang, D. R. Snead, I. A. Cree, and N. M. Rajpoot, "Locality sensitive deep learning for detection and classification of nuclei in routine colon cancer histology images," *IEEE transactions on medical imaging*, vol. 35, no. 5, pp. 1196–1206, 2016.
- [39] P. Kisilev, E. Sason, E. Barkan, and S. Hashoul, "Medical image description using multi-task-loss cnn," in *Deep Learning and Data Labeling for Medical Applications*. Springer, 2016, pp. 121–129.
- [40] S. Ren, K. He, R. Girshick, and J. Sun, "Faster r-cnn: Towards real-time object detection with region proposal networks," in *Advances in neural information processing systems*, 2015, pp. 91–99.

- [41] F. Akram, J. Kim, C. Lee, and K. N. Choi, "Segmentation of regions of interest using active contours with SPF function," *Comp. Math. Methods in Medicine*, vol. 2015, pp. 710 326:1–710 326:14, 2015.
- [42] S. Lankton and A. Tannenbaum, "Localizing region-based active contours," *IEEE transactions on image processing*, vol. 17, no. 11, pp. 2029–2039, 2008.